A Tunable Laser Diode With a Photothermally Driven Integrated Cantilever and Related Properties

Hiroo Ukita

***Abstract*—This paper proposes a photothermally driven tunable laser diode (LD). We demonstrate a micromechanically tunable structure using an edge-emitting LD, a trial fabrication for a monolithic integration with a cantilever and LDs, an enhanced design for widening the wavelength tuning range, and wavelength variation experiments. We describe the design of an antireflection layer and a bimorph layer structure cantilever and expect the deflection to exceed half a wavelength by the temperature increase of 100 °C. We also confirm a 23-nm wavelength variation by changing the external-cavity length of the LD, which features an antireflection coating on the LD facet facing the external mirror.**

***Index Terms*—III-V compounds, antireflection coating, bimorph structure, external-cavity length, gallium arsenide (GaAs), indium phosphide (InP), integrated systems, monolithic integration, optical microelectromechanical systems (MEMS), photothermal effect, thermal strain, tunable laser diode (LD), wavelength tuning.**

I. Introduction

EXTREMELY-SHORT external-cavity laser diodes (ESEC LDs) have been demonstrated for monitoring the reflectivity or displacement in micromechanical photonic devices [1]. Optical disk bits are read out in the near field from the difference in medium reflectivity with an antireflection-coated LD and a photodiode (PD) [2].

Tunable LDs can also be demonstrated in an ESEC configuration. They include desirable properties for optical communication, optical data storage, spectroscopy, and a variety of sensing and measuring systems. A vertical cavity surface-emitting LD (VCSEL) or a light-emitting diode (LED) with a micromechanical reflector can be used for tuned devices [3], [4]. The structure is designed to have an air gap of about a wavelength. When a voltage is applied to the membrane reflector, the electrostatic force reduces the air gap, which in turn reduces the wavelength. An edge-emitting LD is also available for micromechanically tunable lasers [5].

In this paper, we have produced a trial fabrication of the semiconductor micro-cantilever (MC) and LDs on a gallium arsenide (GaAs) substrate. The MC (110 μm long) was driven by the light from the integrated LD with a mechanical resonant frequency of 200.6 kHz.

We have also designed the MC structure to widen its deflection to greater than half a wavelength, which is required for the tunable LD at off-resonant frequencies. Furthermore, we have derived an analytical model for a five-layer MC to predict the deflection that occurs due to temperature increase caused by the light from the LD integrated opposite to the tunable LD.

Manuscript received September 26, 2003; revised February 4, 2004.

The author is with the Faculty of Science and Engineering, Ritsumeikan University, Shiga 525-8577, Japan (e-mail: ukita@se.ritsumei.ac.jp).

Digital Object Identifier 10.1109/JSTQE.2004.828474

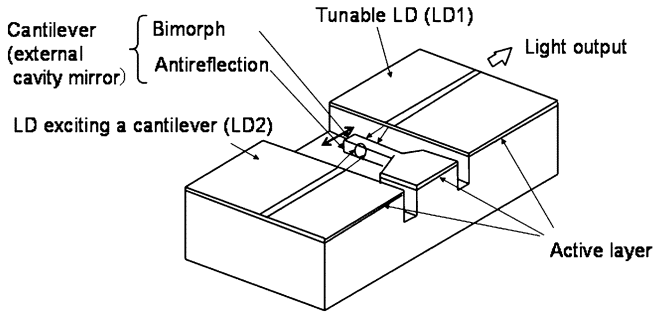

Fig. 1. Structure of a tunable LD, LD1 with an MC driven photothermally by an LD, LD2. The LD1, LD2, and MC are integrated on a GaAs substrate by surface micromachining techniques.

The laser wavelength of the LD can be easily changed by varying the external-cavity length. However, the wavelength variation mechanism for such ESEC LDs has not been clarified till now [6], partly because of the lack of experimental data on the parameters of the external-cavity length, the LD facet reflectivity facing the external mirror, the external mirror reflectivity, and the LD drive current. We experimentally measured and analyzed the effect of the feedback light for various coupled conditions using the LD attached to a flying slider.

In Section II, we have the structure, manufacturing method, and basic characteristics of the proposed device. In Section III, we have the cantilever design for widening the wavelength tuning range. In Section VI, we have the basic wavelength characteristics of an ESEC LD with a separate ESEC LD setup.

II. Proposed Device

One advantage of the optical method in an integrated system is that it is not affected by electromagnetic interference; this factor is especially critical for highly integrated devices. An earlier disadvantage was that the optical technique required lens and fiber systems to guide the light to a PD or a moving mechanism, although recent micromachining technology has made it easy to eliminate these lens and fiber systems, leading to the integration of optics, mechanics and electronics.

A. Structure

Fig. 1 shows the structure of a tunable LD, LD1, with an MC driven photothermally by an LD, LD2. The light emitted from LD2 onto the side wall of the MC is partially absorbed, heating the MC and producing the bending moment. At mechanical resonant frequency, the MC is excited easily due to the thermal stress caused by a pulsed laser beam from LD2. This horizontal vibration varies the external cavity length between the MC wall and the LD1 facet, and there is so little incident light from LD1

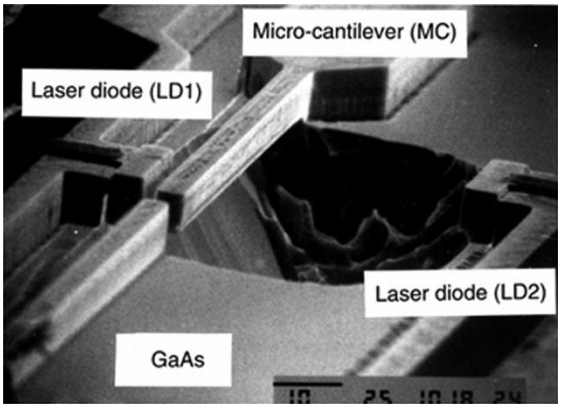

Fig. 2. Photograph of the central part of the tunable LD shown in Fig. 1. The released GaAs–AlGaAs MC was fabricated by undercutting the sacrificial GaAs. The MC length, width and thickness are 110, 3, and 5 μm and the distances from the facet of LD1 to the side wall of the MC and LD2 to MC are 3.0 and 30 μm, respectively.

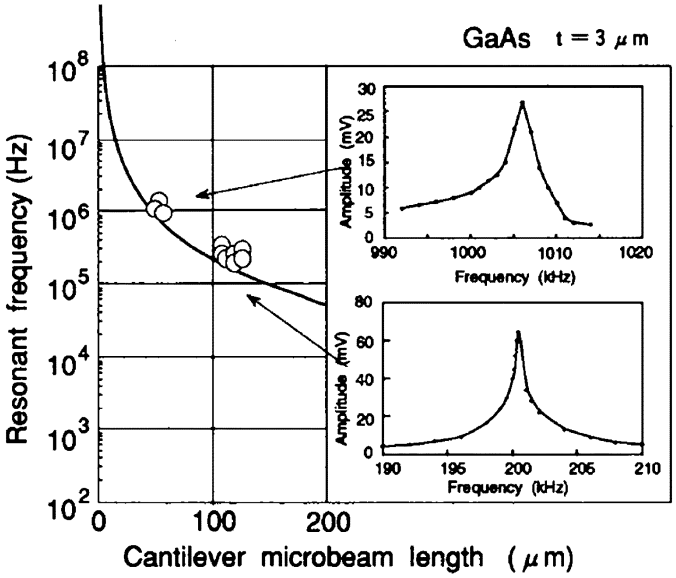

Fig. 3. Mechanical resonant frequency and frequency spectra of the MC integrated with LDs.

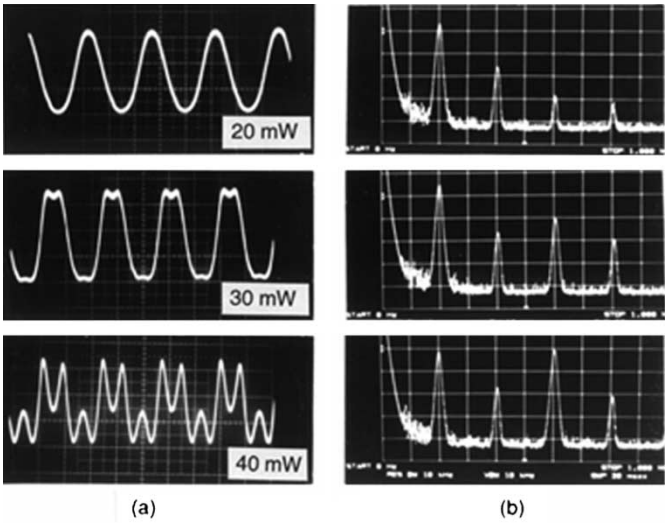

Fig. 4. LD1 light output due to the deflection of the MC caused by the absorbed light from the LD2.

that it has no effect on the MC vibration. The variation of the external cavity length causes the wavelength shift of the LD1.

B. Manufacturing Method

An MC and the LDs were fabricated on a GaAs substrate as shown in Fig. 1. The following are three micromachining processes in fabricating the MC.

1) An etch-stop layer of AlGaAs is formed in the LD structures prepared by metalorganic vapor phase epitaxy (MOVPE).
2) The microstructure shape is precisely defined by a reactive dry-etching technique, which can simultaneously form the vertical etched mirror facets for LDs.
3) A wet-etch window is made with photoresist and the MC is undercut by selective etching to leave the MC freely suspended [7].

These processes are compatible with laser fabrication, so an MC structure can be fabricated at the same time as a LD structure. Furthermore, because a single crystal epitaxial layer carries little residual stress, precise microstructures can be obtained without significant deformation. Fig. 2 shows the main parts of the tunable LD. The hole for wet etching is visible under the MC between LD1 and LD2.

Monolithic integration of optics and micromechanics is possible not only on a GaAs [7] substrate, but also on an indium phosphide (InP) one [8], [9]. A smooth, etched surface and a deep vertical sidewall are necessary for good lasing characteristics of both types of semiconductor microstructures.

C. Basic Characteristics

An LD1, an MC, and an LD2 exciting an MC are integrated on an area of 400×700 μm. The MC was either 110- or 50-μm length, 3 μm wide, 5 μm high. The shorter the MC-LD2 distance, the higher the photothermal conversion efficiency becomes. The LD2's threshold current was 46 mA.

To measure the resonant MC properties, LD2 was lased with the drive current from a functional generator. When the current frequency coincided with the MC mechanical resonant frequency, the amplitude of the power oscillations of the light emitted by LD1 exhibited a maximum. The signal can be obtained by the interference between the LD1 output light and its reflected light from the MC sidewall. Fig. 3 shows mechanical resonant frequency and frequency spectra of the MC. The resonances of the MC for lengths of 110 and 50 μm were 200.6 kHz and 1.006 MHz, respectively.

The signal-to-noise ratio is high (45 dB) due to the lack of mode hop noise owing to the extremely-short (3 μm) external cavity configuration. Fig. 4 shows that the signal amplitude increases as the LD2 light power increases, but an inversion appears in the signal when the MC vibration amplitude becomes greater than $\lambda/4$. The light output varies with a period of $\lambda/2$ as the function of the amplitude of the MC deflection at the mechanical resonant frequency, while the wavelength also varies as the function of the amplitude of the MC deflection.

In a micromechanically tunable LD, the moving part (MC) was integrated with an edge-emitting LD. By varying the external cavity length (MC deflection), the laser wavelength can

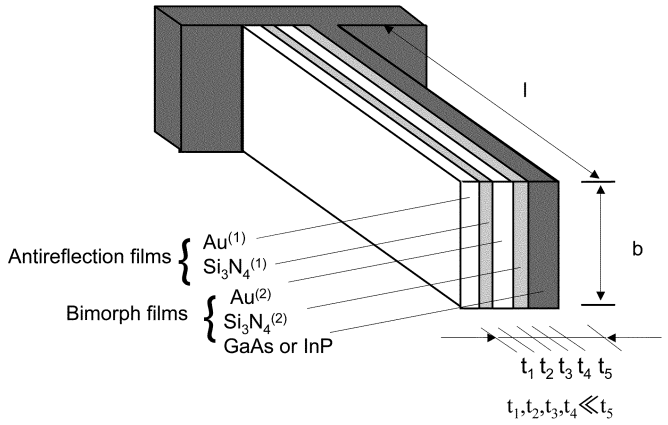

Fig. 5. Schematic drawing of a five-layer MC.

be easily changed. A change of $\lambda/2$ in the external cavity length completes one wavelength tuning cycle in the periodic tuning pattern. Therefore, the MC must move more than $\lambda/2$ even at off-resonant frequencies. Next, we will design the MC structure to satisfy photothermal deflection of greater than half a wavelength.

III. Enlargement of the MC Deflection at Off-Resonant Frequency

GaAs and InP are attractive LD materials for integrating optical and mechanical structures that eliminate the need for optical alignment. When increasing the MC deflection by the temperature increase resulting from the LD light, it is necessary to control the high light absorption rate and the thermal coefficient of expansion of the mismatch sandwiched components. Fig. 5 shows a schematic drawing of a five-layer MC that contains previously mentioned antireflection films and bimorph films.

A. Antirefrection Films

The coefficients $r_{\rm ij}$ and $t_{\rm ij}$ associated with the reflection and transmission at i and j interfaces are given by the Fresnel formula. The formula for $r_{\rm ijk}$ and $t_{\rm ijk}$ for the jth film sandwiched by ith and kth films, are given as follows [10]:

$$r_{\rm ijk} = \frac{r_{\rm ij} + r_{\rm jk}e^{-i2\beta_j}}{1 + r_{\rm ij}r_{\rm jk}e^{-i2\beta_j}} \tag{1}$$

$$t_{\rm ijk} = \frac{t_{\rm ij}t_{\rm jk}e^{-i2\beta_j}}{1 + r_{\rm ij}r_{\rm jk}e^{-i2\beta_j}}. \tag{2}$$

where the perpendicularly incident light phase shift in the jth film is $\beta{\rm j} = 2\pi{\rm d_j}{\rm Nj}/\lambda, N_{\rm j}$ is the complex refractive index, ${\rm d_j}$ is the thickness. Therefore, the total r and t for antireflection films composed of 0 (air), 1 (Au), 2 (Si_3N_4) and 3 (thick Au), are given as

$$r = \frac{r_{012} + z_1 r_{23}e^{-i2\beta_2}}{1 - r_{210}r_{23}e^{-i2\beta_2}} \tag{3}$$

$$t = \frac{t_{012}t_{23}e^{-i2\beta 2}}{1 - r_{210}r_{23}e^{-i2\beta_2}} \tag{4}$$

$$z_1 = t_{012}t_{210} - r_{012}r_{210}. \tag{5}$$

Consequently, the total energy reflectivity R and total energy transmission T are given as:

$$R = rr^* \tag{6}$$

$$T = \frac{N_3}{N_2}tt^*. \tag{7}$$

Fig. 6 shows the total absorption $A\,(=1-R-T)$ and the total reflectivity R of $Au^{(1)}$–$Si_3N_4^{(1)}$–$Au^{(2)}$ versus the $Au^{(1)}$ thickness at the optimal $Si_3N_4^{(1)}$ thickness of 223 nm for the wavelength of (a) 0.83 μm and 366 nm for (b) 1.3 μm. An absorption rate greater than 98% can be attained for both cases. Resulting thicknesses of the five-layer materials are shown in Table I and the properties of the materials are shown in Table II.

B. Five-Layer MC Deflection

The five-layer MC deflection, caused by the thermal stress due to the absorption of the LD light, is analyzed for GaAs and InP by developing the bimetal deflection model [11]. The MC (Fig. 5) is composed of five layers of thickness t_1, t_2, t_3, t_4, t_5, thermal expansion coefficients of $\alpha_1, \alpha_2, \alpha_3, \alpha_4, \alpha_5$, Young's moduli of $\rm E_1, E_2, E_3, E_4, E_5$, a length of l, and a width of b. Temperature distribution within the MC is assumed to be uniform and the temperature change from room temperature to be ΔT.

Fig. 7 shows the deflection of the MC and internal thermal stress due to temperature change. The internal stresses over the cross-section of material i can be reduced to a tensile force P_i and couple moment M_i. Since the internal forces and moments over any cross-section of the MC must be in equilibrium, then

$$P_1 + P_2 + P_3 + P_4 - P_5 = 0 \tag{8}$$

$$\frac{E_1I_1}{r_1} + \frac{E_2I_2}{r_2} + \frac{E_3I_3}{r_3} + \frac{E_4I_4}{r_4} + \frac{E_5I_5}{r_5} - h_1P_1 - h_2P_2 - h_3P_3 - h_4P_4 - h_5P_5 = 0 \tag{9}$$

where $M_i = E_iI_i/r_i, (I_i = {\rm bt}_i^3/12)$ is the moment of inertia, r_i is the radius of curvature of the ith layer of the MC, h_i is the distance between the central plane and ith center plane. The central plane exists between fourth and fifth center plane because of $t_1, t_2, t_3, t_4 \ll t_5$ and $h_4 + h_5 = (t_4 + t_5)/2, h_3 + h_5 = (t_3 + 2t_4 + t_5)/2, h_2 + h_5 = (t_2 + 2t_3 + 2t_4 + t_5)/2, h_1 + h_5 = (t_1 + 2t_2 + 2t_3 + 2t_4 + t_5)/2$.

At the interface between the two layers, the normal strain of the materials must be the same. Therefore,

$$\alpha_1\Delta T - \frac{P_1}{bE_1t_1} - \frac{t_1}{2r_1} = \alpha_2\Delta T - \frac{P_2}{bE_2t_2} + \frac{t_2}{2r_2} \tag{10}$$

$$\alpha_2\Delta T - \frac{P_2}{bE_2t_2} - \frac{t_2}{2r_2} = \alpha_3\Delta T - \frac{P_3}{bE_3t_3} + \frac{t_3}{2r_3}. \tag{11}$$

$$\alpha_3\Delta T - \frac{P_3}{bE_3t_3} - \frac{t_3}{2r_3} = \alpha_4\Delta T - \frac{P_4}{bE_4t_4} + \frac{t_4}{2r_4} \tag{12}$$

$$\alpha_4\Delta T - \frac{P_4}{bE_4t_4} - \frac{t_4}{2r_4} = \alpha_5\Delta T + \frac{P_5}{bE_5t_5} + \frac{t_5}{2r_5}. \tag{13}$$

Here, $r_1 = r_2 = r_3 = r_4 = r_5 = r$ (very thin compared to beam length l) and we derive the curvature $k = 1/r$ by eliminating $P_1, P_2, P_3, P_4, P_5, h_1 = h_2 = h_3 = h_4 = h_5$ and all equations from (8) to (13). Note that the deflection d at the free end of the MC from the curvature k is [12]

$$d = \frac{kl^2}{2} \tag{14}$$

for $1 \ll r$.

Finally, tip deflection of the MC by thermal strain due to the mismatch between the thermal coefficient of the expansion is

$$d = \frac{A}{B} \tag{15}$$

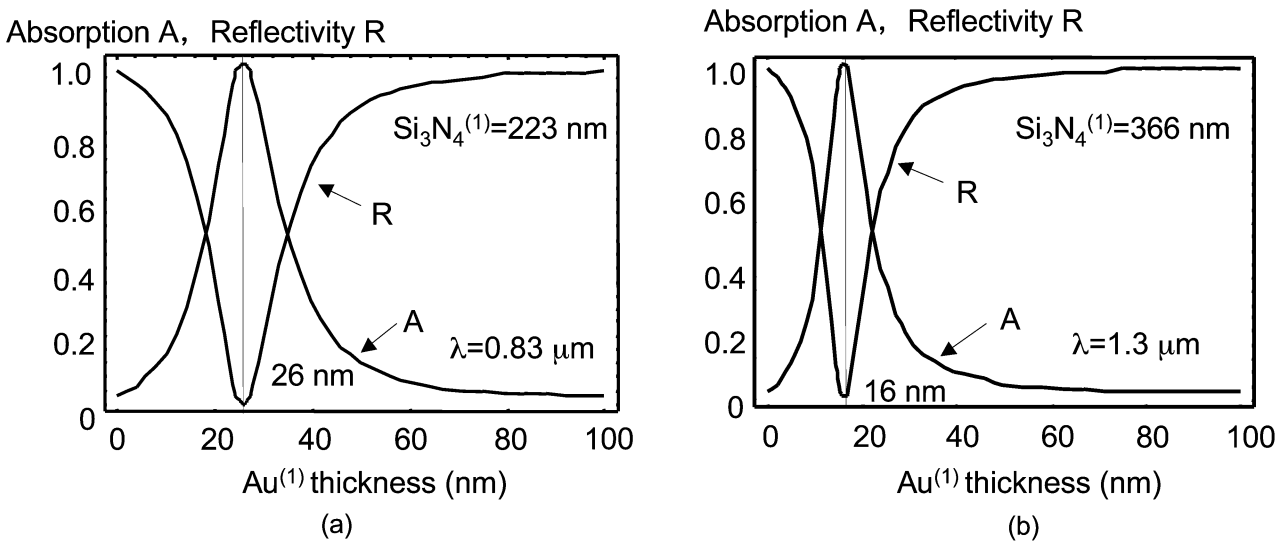

Fig. 6. Total absorption A and reflectivity R of Au–Si_3N_4–Au versus the Au thickness at the optimum Si_3N_4 thickness for wavelengths of (a) 0.83 and (b) 1.3 μm.

TABLE I
DESIGNED MC WITH ANTIREFLECTION AND BIMORPH STRUCTURES

Semiconductor		GaAs	InP
Wavelength (nm)		830	1300
Thickness (nm)	$Au^{(1)}$	26	16
	$Si_3N_4^{(1)}$	223	366
	$Au^{(2)}$	100	100
	$Si_3N_4^{(2)}$	100	100
	Semiconductor	2000	2000
Optical absorption (%)		99	98
Deflection (nm,100 ^{0}C)		486	767
$\lambda/2$ (nm, for reference)		415	650

TABLE II
PROPERTIES OF MATERIALS USED IN FIVE-LAYERED MC

Materials	Thermal expansion coefficient α 10^{-6}/K	Young's modulus E 10^{10}N/m^2 (300K)	Refractive index (830 nm)	Refractive index (1300 nm)
Au	14.2	7.9	0.188+i5.39	0.403+i8.25
Si_3N_4	0.8	0.52	1.5+i0	1.5+i0
GaAs	6.86	8.53	3.67+i0.08	-
InP	4.5	6.07	-	3.205+i0

where

$$
\begin{aligned}
A = 3\Delta T l^2 [&E_1E_2t_1t_2(\alpha_1-\alpha_2)(t_1+t_2)\\
&+E_1E_3t_1t_3(\alpha_1-\alpha_3)(t_1+2t_2+t_3)\\
&+E_1E_4t_1t_4(\alpha_1-\alpha_4)(t_1+2t_2+2t_3+t_4)\\
&+E_1E_5t_1t_5(\alpha_1-\alpha_5)(t_1+2t_2+2t_3+2t_4+t_5)\\
&+E_2E_3t_2t_3(\alpha_2-\alpha_3)(t_2+t_3)\\
&+E_2E_4t_2t_4(\alpha_2-\alpha_4)(t_2+2t_3+t_4)\\
&+E_2E_5t_2t_5(\alpha_2-\alpha_5)(t_2+2t_3+2t_4+t_5)\\
&+E_3E_4t_3t_4(\alpha_3-\alpha_4)(t_3+t_4)\\
&+E_3E_5t_3t_5(\alpha_3-\alpha_5)(t_3+2t_4+t_5)\\
&+E_4E_5t_4t_5(\alpha_4-\alpha_5)(t_4+t_5)]
\end{aligned}
$$

$$
\begin{aligned}
B = 3\,[&E_1E_2t_1t_2(t_1+t_2)^2+E_1E_3t_1t_3(t_1+2t_2+t_3)^2\\
&+E_1E_4t_1t_4(t_1+2t_2+2t_3+t_4)^2\\
&+E_1E_5t_1t_5(t_1+2t_2+2t_3+2t_4+t_5)^2\\
&+E_2E_3t_2t_3(t_2+t_3)^2+E_2E_4t_2t_4(t_2+2t_3+t_4)^2\\
&+E_2E_5t_2t_5(t_2+2t_3+2t_4+t_5)^2+E_3E_4t_3t_4(t_3+t_4)^2
\end{aligned}
$$

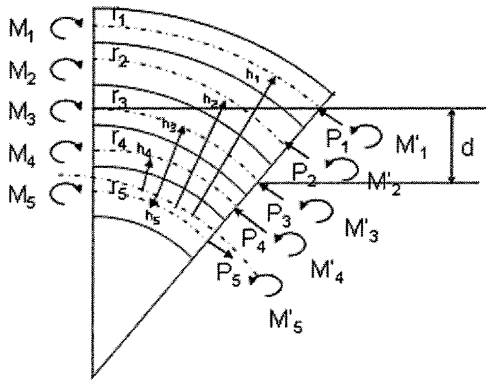

Fig. 7. Deflection of the MC and internal thermal stress due to temperature change.

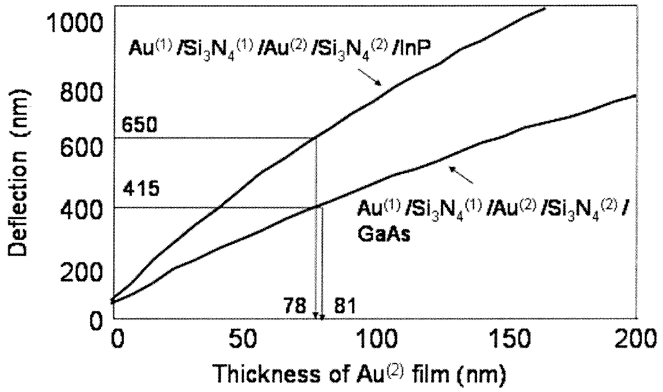

Fig. 8. Deflection of bimorph MCs for $\Delta T = 100\ ^\circ$C with antireflection coating, $Au^{(2)}$ as a parameter.

$$+ E_3E_5t_3t_5(t_3+2t_4+t_5)^2 + E_4E_5t_4t_5(t_4+t_5)^2 + (E_1t_1+E_2t_2+E_3t_3+E_4t_4+E_5t_5) \times \left(E_1t_1^3+E_2t_2^3+E_3t_3^3+E_4t_4^3+E_5t_5^3\right)\Big].$$

Fig. 8 shows the deflection of a five-layer MC with the antireflection films and the bimorph films versus $Au^{(2)}$ thickness, and the semiconductor material as parameters. It can be seen that the deflection greater than $\lambda/2$ is possible when $Au^{(2)}$ is thicker than 81 nm for GaAs ($\lambda = 0.83\ \mu$m) and thicker than 78 nm for InP ($\lambda = 1.3\ \mu$m) LDs. The resulting final five-layer MC design with antireflection and bimorph structures for $\Delta T = 100\ ^\circ$C is summarized in Table I.

IV. Wavelength Variation

Some studies have reported on the wavelength variation for such short-external-cavity LDs based on butt coupling into an optical fiber [6]. However, it was difficult in practice to align the light beam with micrometer-level accuracy. One possible solution is automatic alignment using an air bearing slider. In order to measure the wavelength variation due to the feedback light from the MC under various conditions, we used a semitransparent optical disk mirror and an LD attached on a flying slider.

A. Measurement Method

Fig. 9 illustrates the experimental setup for monitoring the wavelength-related behavior of the LD by the integrated PD, both of which are attached to a flying slider. The InGaAsP–InP LD is isolated from the PD by reactive ion beam etching. The

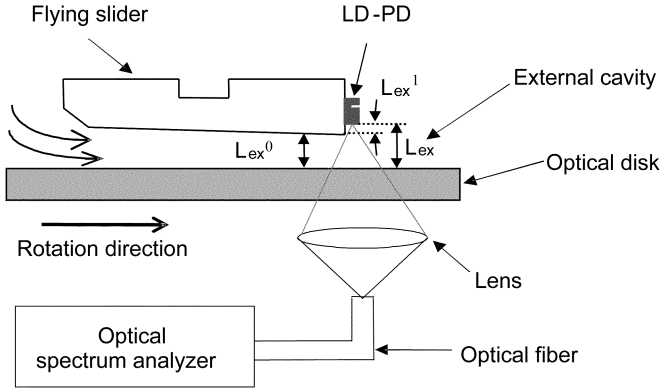

Fig. 9. Setup for the measurement of the wavelength tuning based on ESEC LD attached to an air-bearing slider that flies by air resistance due to disk rotation.

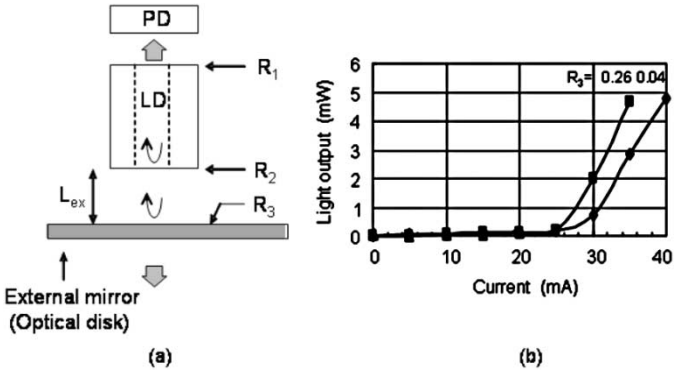

Fig. 10. Representation of the ESEC LD system and its *I–L* characteristics, external mirror reflectivity R_3 as a parameter.

space between LD and PD is about 5 μm and the monitor current sensitivity is 0.1 mA/mW.

Automatic and stable alignment is accomplished by the air bearing, which maintains a spacing $L_{\rm ex}^0$ from submicrometer to several micrometers, depending on the disk velocity. The external cavity length $L_{\rm ex}$ ($=L_{\rm ex}^0+L_{\rm ex}^1$) formed is 2.5 to 4.5 μms long in this experiment, where $L_{\rm ex}^0$ is a flying height depending on the disk velocity and $L_{\rm ex}^1$ is a distance between the LD facet and slider surface.

The light transmitted through the semitransparent optical disk is directed an optical spectrum analyzer through an optical fiber placed opposite to the LD–PD. The laser spectrum is observed with an optical spectrum analyzer with a resolution of 0.1 nm.

The LD coupled with an optical disk forms the same configuration as that of the tunable LD as shown in Fig. 10(a). The laser power variation is monitored by the PD integrated with the LD. Optical feedback is varied by the external cavity length $L_{\rm ex}$ depending on the disk rotation rate, the reflectivity of LD facet facing the optical disk, and the disk reflectivity itself. In the following, the LD facet reflectivity R_1 is 0.32 (cleaved facet), R_2 is 0.01 (antireflection coating), and disk reflectivities R_3 are 0.04 and 0.26.

B. ESEC LD Characteristics

Dependence of lasing characteristics on external-cavity length is described in various parameters: the LD facet reflectivity R_1 facing the PD, the LD facet reflectivity R_2 facing the external mirror, the external mirror reflectivity R_3, and the

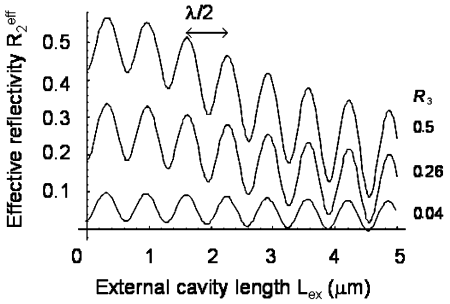

Fig. 11. Dependence of effective reflectivity r_2^{eff} on external-cavity length L_{ex}.

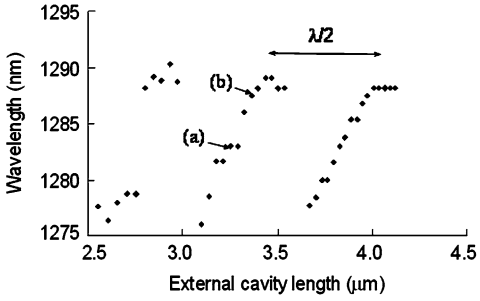

Fig. 12. Dependence of wavelength on external-cavity length L_{ex}, the LD facet reflectivities $R_1 = 0.32, R_2 = 0.01$, the external mirror reflectivity $R_3 = 0.26$, where drive current $I/I_{\text{th}} = 1.6$.

LD drive current. The external-cavity length L_{ex} also affects the coupling coefficient η which is defined by (16) as the ratio between the feedback light power to the original emitted light power, where Gaussian beam waists $(1/\text{e}^2)$ at the LD facet are w_{x0} and w_{y0} and $z = 2L_{\text{ex}}$

$$\eta \equiv \frac{\left|\int\int_{-\infty}^{\infty} E_z E_0\, dx\, dy\right|^2}{\int\int_{-\infty}^{\infty} |E_z|^2\, dx\, dy \int\int_{-\infty}^{\infty} |E_0|^2\, dx\, dy} = \frac{4\sqrt{\left\{1+\left(\frac{\lambda z}{\pi w_{x0}^2}\right)^2\right\}\left\{1+\left(\frac{\lambda z}{\pi w_{y0}^2}\right)^2\right\}}}{\left\{2+\left(\frac{\lambda z}{\pi w_{x0}^2}\right)^2\right\}\left\{2+\left(\frac{\lambda z}{\pi w_{y0}^2}\right)^2\right\}}. \quad (16)$$

Effective reflectivity r_2^{eff} has been successfully introduced as (17) to assist understanding of the external-cavity LD lasing characteristics by replacing the LD facet reflectivity r_2 facing the external mirror

$$R_2^{\text{eff}} = r_2^{\text{eff}} r_2^{\text{eff}^*} = \frac{r_2^2 + a^2 r_3^2 + 2a r_2 r_3 \cos(2\beta_2 L_{\text{ex}})}{1 + a^2 r_2^2 r_3^2 + 2a r_2 r_3 \cos(2\beta_2 L_{\text{ex}})} \quad (17)$$

where N_1 is the refractive index of the internal cavity (LD medium), N_2 is that of the external cavity (air), $r_1 = \sqrt{R_1}, r_2 = \sqrt{R_2}, r_3 = -\sqrt{R_3}$ are the amplitude reflectivities, $\beta_i 2\pi N_i/\lambda$ is the propagation constant, $a(=\sqrt{\eta})$ is the amplitude coupling coefficient for the external-cavity length L_{ex}. For a typical LD, Gaussian beam waists $(1/e^2)$ are 1.3 μm and 2.54 μm, dependence of effective reflectivity r_2^{eff} on external-cavity length L_{ex} is calculated using (16) and (17), as shown in Fig. 11. It is clear from the figure that r_2^{eff} changes every half wavelength $(\lambda/2)$.

We experimentally analyzed how the parameters of the coupling system affect the ESEC LD operation. The light output power coupled to the external mirror depends not only on the ESEC length L_{ex}, but also on the effective reflectivity r_2^{eff}, i.e., reflectivities of the laser facet r_1, r_2, and that of the external mirror r_3. Light output versus drive current (*I-L* characteristics) with an external mirror, constructive in phase, is presented in Fig. 10(b), with $r_1 = 0.32, r_2 = 0.01$, and r_3 as parameters $(r_3 = 0.04, 0.26)$. The threshold current of the ESEC LD with feedback light is reduced according to r_2^{eff}, i.e., by η, r_2, and r_3.

The wavelength also depends not only on the effective reflectivity r_2^{eff}, but also on the external-cavity length L_{ex}. Wavelength tuning and the spectral behavior due to the light feedback is shown in Fig. 12 for an antireflection-coated LD where the drive current (normalized by the threshold current) $I/I_{\text{th}} = 1.6$, reflectivities $r_1 = 0.32, r_2 = 0.01$, and $r_3 = 0.26$. The nonlinear and $\lambda/2$ periodic variation with the external-cavity length

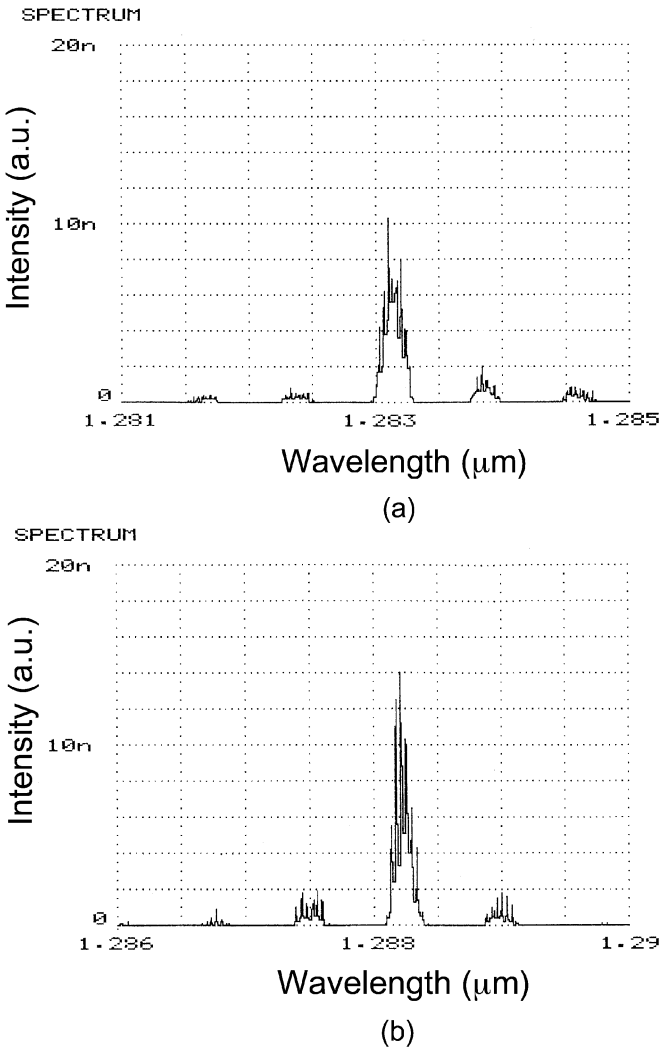

Fig. 13. Spectra at (a) and (b) in Fig. 12.

is known to be caused both by the composite mode selection and the gain spectrum variation due to the light feedback. It can be seen from Fig. 12 that wavelength shift varied every $\lambda/2$, and the total tuning range was 23 nm around 1300 nm, achieved by applying an antireflection coating film on the LD facet facing the external mirror. The spectral structure of the tuned light is shown in Fig. 13(a) and (b), which shows the single modes tuned for the antireflection-coated LD. These results are like those of [6], but details will be published in a separate paper soon.

V. Conclusion

We produced a trial fabrication of a semiconductor MC, edge-emitting LDs on the surface of a GaAs substrate. The MC was shaped by reactive dry-etching and undercut by selective wet-etching, making it free to vibrate. The MC was 3 μm wide, 5 μm high, and either 110 or 50 μm long and driven photothermally with the mechanical resonant frequencies of 200.6 kHz or 1.006 MHz, respectively. The wavelength varies according to the MC deflection.

We designed a five-layer MC for a GaAs and an InP substrate to widen the wavelength variation of the LD at off-resonant frequencies. In the case of the GaAs, the designed MC consists of a 26-nm gold layer/223-nm Si_3N_4 dielectric antireflection layer/100-nm gold layer/100-nm Si_3N_4 dielectric bimorph layer, and a 2-μm-thick GaAs layer. We expect that the MC tip deflection is greatly enhanced to exceed half a wavelength, which is required for a tunable LD.

Finally, we experimentally analyzed how the parameters of the coupling system affect the ESEC LD operation by using a rotating optical disk and an LD attached to a flying slider. The parameters included the reflectivities of the LD facets, the reflectivity of the external mirror, and the LD drive current. We confirmed a 23-nm tuning range around a wavelength of 1.3 μm by changing the external-cavity length for the LD with an antireflection coating on the facet facing the external mirror.

From these results, we believe that by employing the MC design and the fabrication method described earlier, a photothermally driven micromechanical tunable LD will be available in the future.

Acknowledgment

The author would like to thank Dr. Y. Uenishi of NTT for the fabrication of ESEC LDs and graduate students Y. Masuda, Y. Tanabe, A. Okada, and Y. Karaki of Ritsumeikan University for their help with the experimental and theoretical analyses.

References

[1] H. Ukita, "Micromechanical photonics," *Opt. Rev.*, vol. 4, pp. 623–633, 1997.

[2] K. Kataja, J. Aikio, and G. How, "Numerical study of near-field writing on a phase-change optical disk," *Appl. Opt.*, vol. 41, no. 10, pp. 4181–4187, 2002.

[3] M. C. Larson and J. S. Harris, "Wide and continuous wavelength tuning in a vertical-cavity surface-emitting laser using a micromachined deformable-membrane mirror," *Appl. Phys. Lett.*, vol. 68, pp. 891–893, 1996.

[4] F. Sugihwo, M. C. Larson, and J. S. Harris, "Simultaneous optimization of membrane reflectance and tuning voltage for tunable vertical cavity lasers," *Appl. Phys. Lett.*, vol. 72, pp. 10–12, 1998.

[5] Y. Uenishi, M. Tsugai, and M. Mehregany, "Hybrid-integrated laser-diode micro-external mirror fabricated by (110) silicon micromachining," *Electron. Lett.*, vol. 31, pp. 965–966, 1995.

[6] Y. Sidorin and D. Howe, "Laser diode wavelength tuning based on butt coupling into an optical fiber," *Opt. Lett.*, vol. 22, pp. 802–804, 1997.

[7] Y. Uenishi, H. Tanaka, and H. Ukita, "AlGaAs–GaAs micromachining for monolithic integration of micromechanical structures with laser diodes," *IEICE Trans. Electron.*, vol. E78-C, no. 2, pp. 139–145, 1995.

[8] K. Hjort, K. Streubel, and P. Viktorovitch, "Indium phosphide based micro optoelectro mechanics," in *Summer Topical Meet. Optical Micro Electro Mechanical Systems and Their Applications*, 1996, Keystone, 96TH8164, p. 45.

[9] M. W. Pruessner, T. T. King, D. P. Kelly, R. Grover, L. C. Calhoun, and R. Ghodssi, "Mechanical property measurement of InP-based MEMS for optical communications," *Sens. Actuators A, Phys.*, vol. 105, pp. 190–200, 2003.

[10] M. Born and E. Wolf, *Principles of Optics*. Oxford, U.K.: Pergamon, 1970, p. 62.

[11] W.-H. Chu, M. Mehregany, and R. L. Muller, "Analysis of tip deflection and force of a bimetallic cantilever microactuator," *J. Micromech. Microeng.*, vol. 3, pp. 4–7, 1993.

[12] J. M. Gere and S. P. Timoshenko, *Mechanics of Materials*. Boston, MA: PWS-Kent, 1990, p. 301.

Hiroo Ukita was born in Matsuyama, Japan, on Augest 28, 1945. He received the Dr. Eng. degree from Tohoku University, Sendai, Japan, in 1973.

He joined Nippon Telegraph and Telephone Corporation in 1973, where he worked in the field of optical recording and optical MEMS. Since 1995, he has been with Ritsumeikan University, Shiga, Japan, serving as a Professor with the Faculty of Science and Engineering. His current interests include optical tweezers and optical microsystems with the integration of photonics and mechanics.

Prof. Ukita received the 1990 Best Paper Award at the Optical Memory Symposium and also received the 1994 Precision Engineering Award from the Japan Society for Precision Engineering. He is a member of the IEEE Laser and Electro-Optics Society, American Association for the Advancement of Science, Optical Society of Japan, Laser Society of Japan, Japan Society of Applied Physics, Japan Society for Precision Engineering, and the Institute of Electronics, Information and Communication Engineers of Japan. Since 1987, he has worked for the Committee of the International Symposium on Optical Memory and currently serves on the editorial board of the Optical Society of Japan and *Smart Materials and Structures*.